Numerical solution of moving boundary problems in diffusion processes with attractive and repulsive interactions

2002 J. Phys. A: Math. Gen. 35 1575

(http://iopscience.iop.org/0305-4470/35/7/307)

INSTITUTE OF PHYSICS PUBLISHING JOURNAL OF PHYSICS A: MATHEMATICAL AND GENERAL

J. Phys. A: Math. Gen. **35** (2002) 1575–1588 PII: S0305-4470(02)22224-6

Numerical solution of moving boundary problems in diffusion processes with attractive and repulsive interactions

A P Reverberi[1], **E Scalas**[2,3,4] **and F Vegliò**[1]

[1] DIChePP, University of Genova, via Opera Pia 15, 16145 Genova, Italy
[2] Department of Advanced Sciences and Technology, East Piedmont University, Corso Borsalino, 54, I-15100 Alessandria, Italy
[3]Istituto Nazionale di Fisica Nucleare, sezione di Torino, via P Giuria 1, 10125 Torino, Italy

Received 29 January 2001, in final form 29 September 2001
Published 8 February 2002
Online at stacks.iop.org/JPhysA/35/1575

Abstract

A moving boundary problem modelling a diffusion-limited reaction in the presence of a nonlinear diffusivity is studied in this paper. The equations are solved by means of a front-tracking method with proper regularizing techniques. Reliable results are obtained in the case of both attractive and repulsive interactions between the diffusing species. We investigate the effects of the two kinds of interaction and their relevant strength on the width of concentration profiles into the unreacted zone and the value of the unknown at the moving interface.

The results are discussed in connection with Monte Carlo simulations of on-lattice models and with some experimental observations.

PACS numbers: 02.60.Lj, 02.70.Bf, 61.43.Hv, 68.35.Fx, 82.40.Ck

1. Introduction

Moving boundaries have received great attention in many fields of research. In particular, we point to some studies concerning applied mathematics and the theory of estimates in heat and mass transfer operations [1–4] as well as in interface dynamics of pattern forming systems [5–7]. Among them, viscous fingering in fluid mechanics and dendritic growth equations in condensed matter physics have long been objects of intense investigation; moreover, phenomena in other interdisciplinary fields such as dielectric breakdown fronts in gases [8, 9] have many elements in common with the aforementioned studies.

Interesting questions appear when a generation term overlaps with a pure diffusion [10–14]. This is true not only in the context of pure physics, but also for the applied literature [15–18]. Various discrete models have been proposed to investigate reaction–diffusion

[4] Corresponding author.

processes with Monte Carlo simulations [19–22]; the patterns often show anomalous geometries and scaling laws in interface dynamics. In this case, continuum models are generally expressed in the following form:

$$\frac{\partial \underline{u}}{\partial t} = D\nabla^2 \underline{u} + \underline{F}(\underline{u}, t) \tag{1}$$

where $\underline{u}$ is a set of dependent variables, D is a matrix of diffusivities and $\underline{F}$ is a vector related to chemical reaction kinetics. Several attempts have been made to find solutions of equation (1) for some classes of F functions in one spatial dimension. Particular attention has been given to the asymptotic behaviour of front speed [23, 24]. Localization or de-localization of reaction fronts may occur according to the specific rules governing the contact between the initially separated interacting species; the direction of the front motion is controlled by a parameter depending on the initial particle densities and on the relevant diffusivities [25]. In particular, the long-time behaviour of the front width w at criticality follows the power law $w \sim t^{\beta}$ with $\beta = 1/6$ in the case of a characteristic binary reaction with second-order kinetics [26].

In this work, we consider a reaction–diffusion process in a diffusion-limited regime with a concentration-dependent diffusion coefficient $D(u)$. This choice is somewhat different from equation (1). We are also interested in the short- and long-time behaviour of the unknown $u(x, t)$.

The solution of the so-called 'full time-dependent free boundary problems' [27] is based on several techniques trying to give reliable results even in critical situations derived from sharp boundaries and anisotropies [28]. The phase-field approach relies upon a modelling of moving interfaces with a continuum approximation; it is supposed that the transition from one phase to another gradually occurs in a space of finite width δ, where a field parameter varies smoothly between the limiting values, constant in each phase. This approach, like the front-fixing [29] and spectral techniques [30], does not show the unphysical numerical oscillations typical of the front-tracking methods. In the latter techniques, the interface position $s(t)$ and the value of the unknown $u[s(t)]$ at the moving interface are updated at every time step; the problem is intrinsically nonlinear despite the linearity of the diffusion equation [31].

Several variants of the front-tracking methods exist; fixed and adaptive grid mesh techniques and the method of lines are most commonly used in the literature. In the method of lines, the moving boundary problem is solved transforming the PDEs contained in the model into a set of ODEs, which are solved at discrete times or at discrete space points [32]; moreover these techniques, like the front-fixing methods, often require some variable transformations that may add further algebraic complication to a problem that can be, even originally, tricky.

Here, we use a front-tracking method that, though traditional in its essence, is implemented with some useful regularizing criteria, eliminating the drawbacks outlined above.

The paper is organized as follows. In section 2, we describe the model and give some details of the numerical recipe adopted to regularize the solution; in section 3 we present the results with a particular attention to the correlation between this approach, the discrete models dealing with diffusion fronts in case of particle interactions and some experimental observations. In section 4, we investigate a perturbative solution of the problem with concentration-dependent diffusivity and we relate the analytical results to those derived from the numerical approach. In section 5 we draw the conclusions and trace the direction for future work.

2. Model and algorithm

We shall consider here a moving boundary problem of the following kind:

$$\frac{\partial u}{\partial t} = \frac{\partial}{\partial x}\left[D(u)\frac{\partial u}{\partial x}\right] \tag{2}$$

$$\frac{\mathrm{d}s}{\mathrm{d}t} = f(u)\left.\frac{\partial u}{\partial x}\right|_{x=s} \tag{3}$$

where u is the unknown variable assuming a specific role according to the relevant physics of the process. For instance, u can represent the mole fraction or adimensional temperature in the case of mass or heat transport, respectively. In the examples that will be considered, we shall refer only to mass transport and u will be treated as concentration in the following. $f(u)$ is a known function describing transport across the moving interface $s(t)$; the position of the interface is an unknown to be determined together with the profile of u in the semi-infinite medium; x and t are space and time variables and $D(u)$ is a nonlinear expression of the diffusion coefficient depending on concentration.

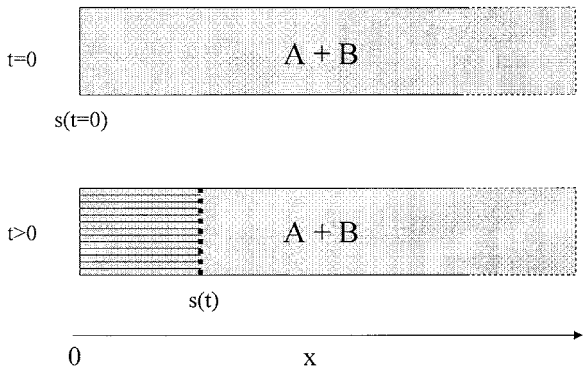

Figure 1. Scheme of the semi-infinite medium described in the paper. The upper rectangle refers to an initial situation of mixed components with uniform concentration of both the diffusing species A and the inert component B; the lower one is a snapshot of the reaction in progress. The dotted interface moves rightwards and the hatched area to the left of it indicates the region where A has already been depleted.

The above system can model a reaction–diffusion process schematically illustrated in figure 1. At $t = 0$, a one-dimensional space region ($x > 0$) is filled by two chemical species A and B with a given concentration. Only A is subject to a chemical reaction with another species C, which enters the medium at $x = 0$ and annihilates the component A according to the scheme A + C = D. For instance, C might be a gaseous component diffusing by cation vacancies into a solid phase A + B and forming a binary compound with A only, as supposed in Wagner's pioneering work [33].

The kinetic rate of the reaction is supposed to be infinite; therefore, only the diffusion process of A in the zone not affected by the reaction governs the advancing of the front.

At $t > 0$, the picture of this reaction–diffusion process is characterized by

(a) a region $\{0 < x < s(t)\}$ with B and D, where A has been chemically depleted and
(b) a region $\{x > s(t)\}$ with A + B, where we have to determine the concentration profile of the diffusing species and its value at the moving interface taking into account a specific expression of the diffusivity $D(u)$.

For the present simulations, we interpret u as the concentration of the component A whose diffusivity is chosen as follows:

$$D(u) = D_0 \exp\left(\alpha \frac{u - \bar{u}_0}{\bar{u}_1 - \bar{u}_0}\right). \tag{4}$$

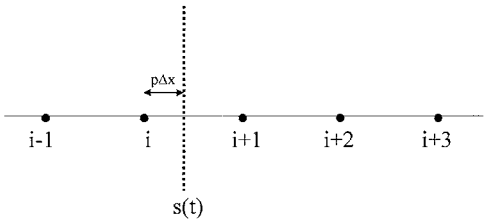

Figure 2. Scheme of the spatial discretization technique adopted in the method here outlined.

An exponential law in the expression of $D(u)$ has been commonly adopted in the literature [34]. D_0 is a constant reference value; α is a parameter that modulates the attractive or repulsive A–A particle interaction defined by

$$\begin{aligned} &\alpha > 0 \rightarrow \frac{\mathrm{d}D}{\mathrm{d}u} > 0 \rightarrow \text{ repulsive interaction} \\ &\alpha < 0 \rightarrow \frac{\mathrm{d}D}{\mathrm{d}u} < 0 \rightarrow \text{ attractive interaction.} \end{aligned} \tag{5}$$

u_0 and u_1 are constants appearing in the boundary and initial conditions:

$$\begin{aligned} &t = 0 \qquad u(x,0) = \bar{u}_1 \qquad x > 0 \\ &t, x = 0 \qquad u(0,0) = \bar{u}_0 \\ &x \rightarrow \infty \qquad \frac{\partial u}{\partial x}(x,t) = 0 \qquad t > 0. \end{aligned} \tag{6}$$

Few analytical solutions of the system (2), (3) are known in closed form, and they concern cases where D is constant for some given expression of $f(u)$. These exact solutions are usually presented as functions of the scaled variable $\xi = \frac{x}{t^{1/2}}$ and are called similarity solutions.

The front-tracking method here adopted is based on a fixed-grid technique; the solution $\bar{u}_{i,j}$ of the system (2), (3) at grid point $i\Delta x$ for time $j\Delta t$ is approximated by a sequence of functions $\{u^n\}$ with $\operatorname{Lim}_{n\to\infty} u^n_{i,j} = \bar{u}_{i,j}$. For points lying far from the moving interface, a standard Crank–Nicolson code can be used to discretize equation (2) as follows:

$$\begin{aligned} \tfrac{1}{2}\left(u_{xx}|_{i,j+1} + u_{xx}|_{i,j}\right) = \Phi \Bigg(& i\Delta x, (j+\tfrac{1}{2})\Delta t, \tfrac{1}{2}(u_{i,j+1} + u_{i,j}), \tfrac{1}{2}\left(u_x|_{i,j+1} + u_x|_{i,j}\right), \\ & \frac{1}{\Delta t}(u_{i,j+1} - u_{i,j}) \Bigg) \end{aligned} \tag{7}$$

where Φ is a nonlinear operator depending on the lower-order derivatives by which the Laplacian contained in (2) is expressed, that is

$$\Phi = \Phi\left(x, t, u, \frac{\partial u}{\partial x}, \frac{\partial u}{\partial t}\right). \tag{8}$$

A typical scheme capturing the essential features of the method is discussed in [35], where it is shown how to minimize the effect of a discontinuity in the concentration values at the starting interface in a simple linear case. Moreover, we used another regularizing criterion that, due to its basic role in the reliability of the method, is worth recalling briefly.

Given some Δx value in the space grid mesh, the position of the moving interface will be usually located between two neighbouring grid points i and $i+1$ at any time $j\Delta t$, say:

$$s(j\Delta t) = (i + p)\Delta x \qquad 0 < p < 1. \tag{9}$$

A grid crossing at point $i+1$ occurs when (see figure 2)

$$s(j\Delta t) < (i+1)\Delta x < s[(j+1)\Delta t]. \tag{10}$$

This is a particularly critical situation as

$$\operatorname*{Lim}_{s\to(i+1)\Delta x^-} u(s) \neq \operatorname*{Lim}_{s\to(i+1)\Delta x^+} u(s). \tag{11}$$

The origin of the above discontinuity lies in the expression of the Lagrange interpolation formulae [29] by which the spatial derivative present in (3) is discretized in the classical method. Applying this formalism in the neighbourhood of the moving boundary and restricting the expansion to n fixed grid points, one obtains

$$\begin{aligned}\left.\frac{\partial u}{\partial x}\right|_{x=s} &= Q_0(s, x_{i+1}, \ldots, x_{i+n})u(s) + \sum_{k=1}^{n} Q_k(s, x_{i+1}, \ldots, x_{i+n})u(x_{i+k}) \\ &= \Psi(s, x_{i+1}, \ldots, x_{i+n})\end{aligned} \tag{12}$$

where Q_k are rational functions of polynomials having singularities when $s \to x_{i+k}$ for at least one k. This is the cause of the numerical oscillations previously described leading to unphysical results and even divergence in some cases. The problem can be overcome by means of a regularizing technique [36] based on proper weights cutting off the singularities, damping the spurious oscillations and preserving the second-order accuracy in space and time required by the Crank–Nicholson method. Many stable algebraic expressions alternative to (12) can be chosen. When we use a forward expansion, that is for $\{x_n > s, \forall n\}$, a suitable n-point code for the marching interface can be written as

$$\left.\frac{\partial u}{\partial x}\right|_{x=s} = \frac{x_{i+1}-s}{\Delta x}\Psi(s, x_{i+1}, \ldots, x_{i+n}) + \frac{s-x_i}{\Delta x}\Psi(s, x_{i+2}, \ldots, x_{i+n+1}). \tag{13}$$

For the present simulations, we used an expression for $f(u)$ of the type

$$f(u) = \frac{D(u)}{1-u}; \tag{14}$$

this corresponds to a Fickian mass transport law across the interface without any change in bulk density. Such an expression has been adopted [34] in the case of concentration-dependent or independent diffusivity.

3. Results and discussion

In figure 3, the time trend of the interface position $s(t)$ is considered. Three scatter graphs are reported in the case of repulsive, zero and attractive interactions. As expected, we find no deviations from the classical 'parabolic' law of the moving front, that is $s(t) = kt^{\beta}$ with $\beta = 0.5 \pm 0.05$. We point out that, in all the simulations, we considered at most values of α that produced variation of $D(u)$ corresponding to a range of more than two orders of magnitude in the global manifold $x > s(t)$. The pre-exponential factor k is affected by the kind and extent of interactions [37]; the effects induced on the front speed result in a faster motion in the case of repulsive interaction. This phenomenon will be reconsidered later when we discuss some interesting features of experimental data.

In figure 4, the concentration profiles for $x > s(t)$ are plotted for fixed times in order to compare the non-correlated case ($\alpha = 0$) with the attractive one. For all the x values at which both the profiles exist at time $\bar{t}$, that is for $x > \max\{s(\bar{t}, \alpha > 0); s(\bar{t}, \alpha = 0)\}$, the concentration values for the attractive interactions are greater than those pertaining to the non-correlated case, namely

$$u(x, \bar{t}, \alpha < 0) > u(x, \bar{t}, \alpha = 0). \tag{15}$$

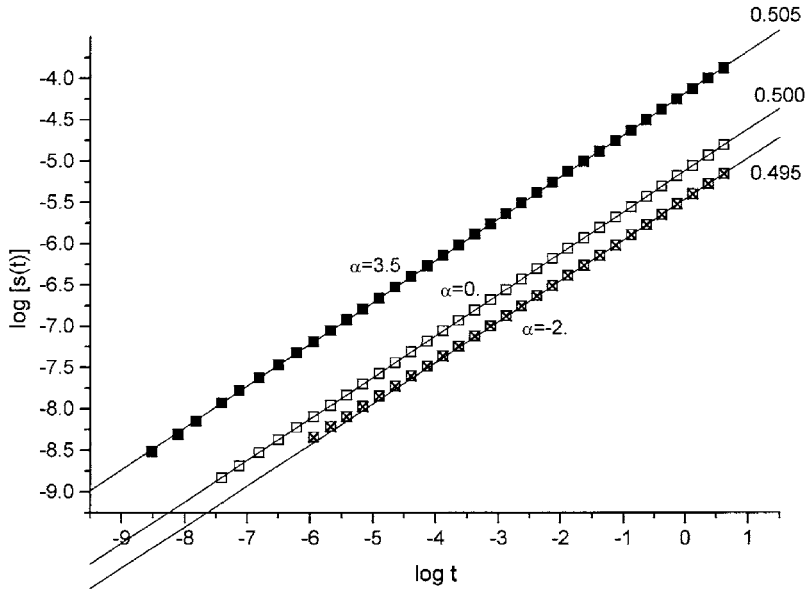

Figure 3. Double-logarithmic plot of the interface position $s(t)$ versus time. Three scatter graphs are reported for different values of the parameter α, which decreases from top to bottom. All values are obtained with $D_0 = 10^{-4}$, $\bar{u}_1 = 0.5$ and $\bar{u}_0 = 2.2 \times 10^{-2}$.

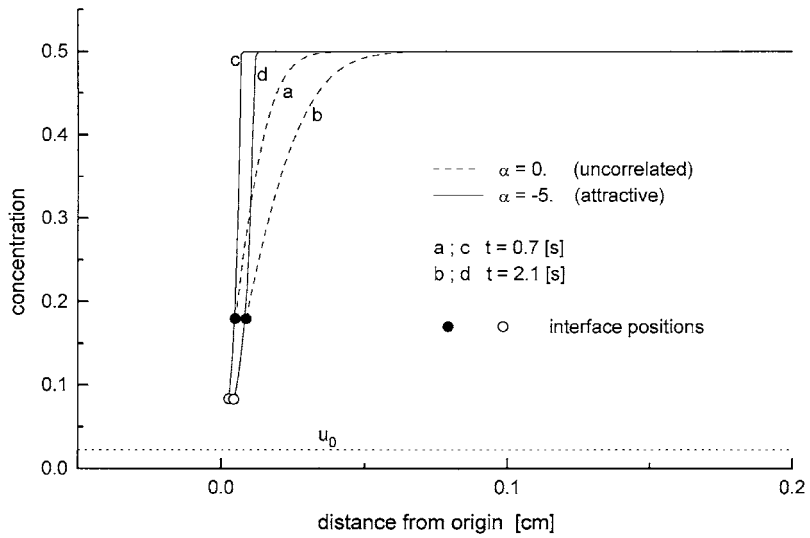

Figure 4. Plot of concentration profiles of A as a function of x. Solid lines and open circles refer to attractive interactions ($\alpha < 0$), dashed curves and solid circles to null interaction ($\alpha = 0$). Circle abscissas indicate interface positions in all cases. D_0, $\bar{u}_1$ and $\bar{u}_0$ are as in figure 3.

Despite this fact, it is interesting to note that the concentration $u[s(t, \alpha)]$ at the moving interface subject to attractive interactions is significantly lower than in the constant-diffusivity (non-correlated) case; that is,

$$u[s(\bar{t}, \alpha < 0)] < u[s(\bar{t}, \alpha = 0)]. \tag{16}$$

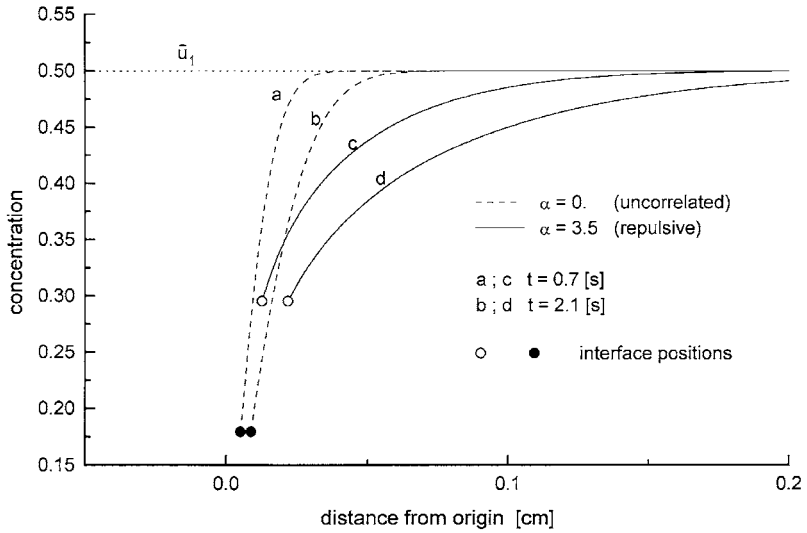

Figure 5. Plot of concentration profiles of A as a function of x. Solid lines and open circles refer to repulsive interactions ($\alpha > 0$), dashed curves and solid circles to null interaction ($\alpha = 0$). Circle abscissas indicate interface positions in all cases. D_0, $\bar{u}_1$ and $\bar{u}_0$ are as in figure 3.

Figure 5 represents a situation which is the opposite of what has been just described. Here, in fact, the case $D = \text{const}$ is compared with the diffusion trend generated by repulsive correlations. Both inequalities (15) and (16) are inverted. In particular we focus our attention on concentration values on the moving interface $s(t, \alpha)$. These values are reconsidered in figure 6, with the only difference that, now, they are plotted as a function of time. The trend for $\alpha = 0$ is also added for the sake of completeness, in order to show the fairly good approximation to the analytical solution that, for this particular case, is well known [33] and is plotted as a dotted line. In the cases considered, for both attractive and repulsive interactions, the concentration values on the moving interface converge to a constant value; the convergence is very rapid for $\alpha > 0$ but becomes considerably slower for $\alpha < 0$. This trend can be observed in the plot for $\alpha = -5$, where we notice a transient deviation from the constant value at short times. Besides, for all values of α that we used in the simulations, we can conclude that

$$\frac{\partial\{u[s(t,\alpha)]\}}{\partial\alpha} > 0 \qquad \text{with} \quad u[s(t,\alpha)] \in \{\bar{u}_0, \bar{u}_1\}. \tag{17}$$

This amounts to saying that, for strong repulsive interactions, the concentration value at the moving interface monotonically approaches the value u_1 of the unperturbed phase for $x \to \infty$, whilst for strong attractive interactions it approaches the starting initial value u_0 corresponding to a very low concentration of A.

The results presented here are independent of the space and time discretization parameters Δx and Δt. Figure 7 reports the concentration profiles at fixed time for attractive ($\alpha = -1$) and repulsive interactions ($\alpha = 1$) versus the space variable x. All plots for different values of Δx and Δt collapse onto a single curve. Figure 8 reports the moving interface concentration versus time for the same values of α. Again, it is shown how the curves overlap with one another for different choices of Δx and Δt.

In the excellent lecture note of van Saarloos [31], it was remarked that neither the concept nor the meaning of the word 'interface' is universally accepted. From this point on, to avoid

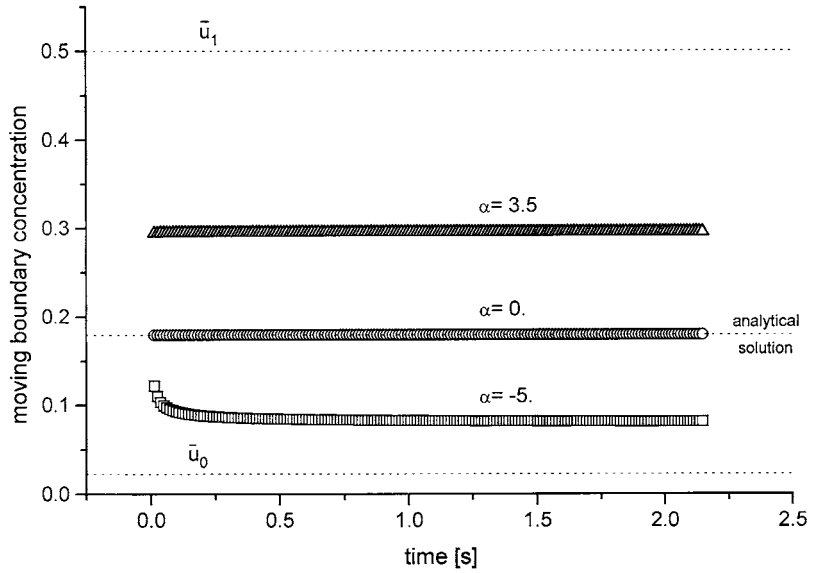

Figure 6. Trend of the moving boundary (interface) concentration versus time for three different values of the parameter α. Dotted lines represent, from top to bottom, the unperturbed value $\bar{u}_1$ for $x \to \infty$, the constant analytical solution for $\alpha = 0$ (taken from [33]) and the initial starting value $\bar{u}_0$, respectively.

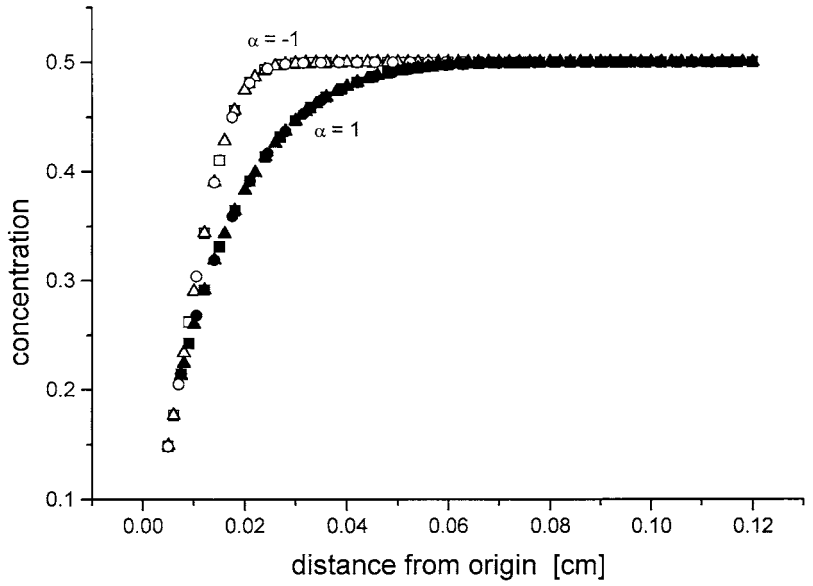

Figure 7. Plot of the concentration profiles at fixed time $t = 1$ for attractive ($\alpha = -1$; open symbols) and repulsive ($\alpha = 1$; solid symbols) interactions versus the space variable x. Triangles, $\Delta x = 5 \times 10^{-5}$; $\Delta t = 5 \times 10^{-5}$; squares, $\Delta x = 10^{-4}$; $\Delta t = 10^{-4}$; circles, $\Delta x = 5 \times 10^{-4}$; $\Delta t = 5 \times 10^{-4}$.

misunderstanding, we shall consider as 'interface' the physical separation located at $s(t)$ dividing two different phases and as 'diffusion front' the zone belonging to the unreacted phase

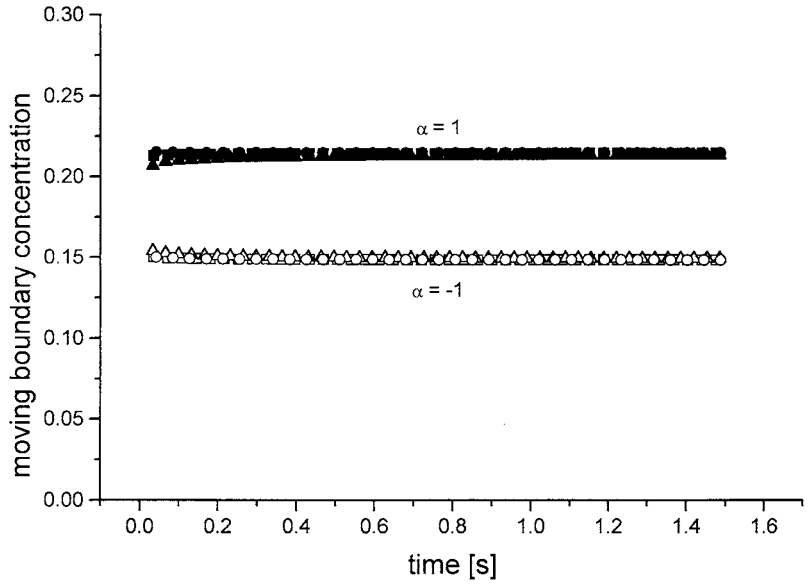

Figure 8. Plot of the moving boundary concentration versus time for attractive ($\alpha = -1$; open symbols) and repulsive ($\alpha = 1$; solid symbols) interactions. Triangles, $\Delta x = 5 \times 10^{-5}$; $\Delta t = 5 \times 10^{-5}$; squares, $\Delta x = 10^{-4}$; $\Delta t = 10^{-4}$; circles, $\Delta x = 5 \times 10^{-4}$; $\Delta t = 5 \times 10^{-4}$.

with $x > s(t)$ whose width σ and medium abscissa $\langle x \rangle$ are defined by the following relations:

$$\langle x \rangle = \frac{\int_{u[s(t,\alpha)]}^{\bar{u}_1} x(u)\,\mathrm{d}u}{\bar{u}_1 - u[s(t,\alpha)]} \qquad \sigma = \sqrt{\frac{\int_{u[s(t,\alpha)]}^{\bar{u}_1} (x - \langle x \rangle)^2\,\mathrm{d}u}{\bar{u}_1 - u[s(t,\alpha)]}}. \tag{18}$$

The discrete approach to diffusion problems has been investigated in detail. Particles generated on a fixed source invade a semi-infinite lattice of initially empty sites with a diffusion motion depending on hard-core exclusion rules in two dimensions. In that framework, particle interactions are modelled introducing various criteria such as nearest-neighbour jump-dependent rates [38] or dipolar potential correlations [39]. The probability densities of occupied sites at fronts generated in a gradient percolation are used to deduce exact values of the percolation threshold p_c. It has also been shown that p_c increases or decreases for repulsive or attractive interactions, respectively [38]. The same trend can be observed (figure 9) in the behaviour of $u(\langle x \rangle, \alpha)$. The results presented in figure 9 are consistent with the behaviour of front concentration values in a gradient percolation process with a moving absorbing wall at constant concentration located at the interface $s(t)$.

Besides, the geometries of fronts in discrete models show a sharp profile for very low α down to the limit of the spinodal transition, whilst for large $\alpha > 0$ characteristic chequer-board patterns with overhangs and ravines appear when the diffusion front becomes larger up to the limit of the order–disorder transition.

Figure 10 shows the influence of the interaction parameter α on the width of the diffusion front σ. The curves are shifted to higher values of σ as α grows, in agreement with the results of the aforementioned on-lattice simulations. Moreover, if we merge the results of figures 4, 5 and 10 with the statements (17), we can make further considerations: for $\alpha \ll 0$, we have $\sigma \approx 0$ and we note the onset of a moving depletion layer, very poor in component A, into the unreacted zone for $x > s(t)$. This corresponds to the limit of the spinodal transition in discrete models. In the opposite case, for $\alpha \gg 0$, we observe a zone where $\nabla x \approx 0$ for $|x - \langle x \rangle| < \sigma$. The

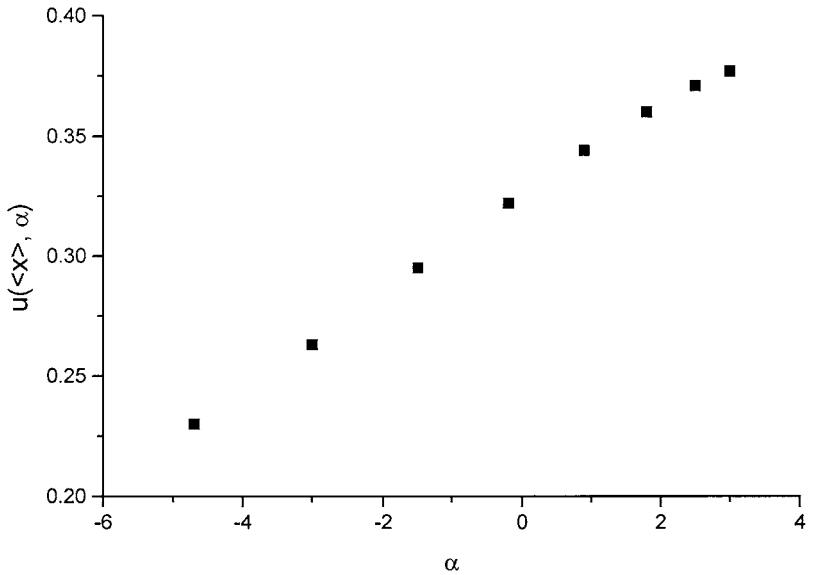

Figure 9. Plot of the concentration value at the diffusion front average position $\langle x \rangle$ versus the interaction parameter α.

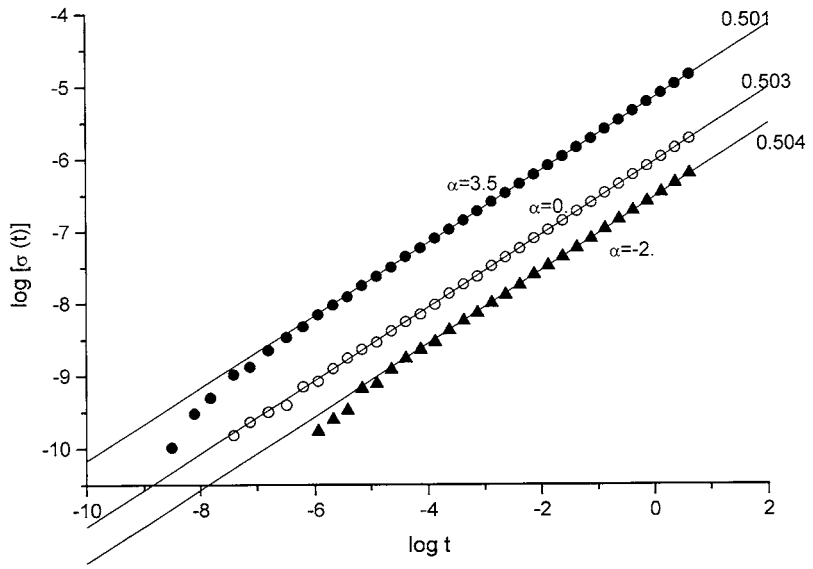

Figure 10. Plot of the width of the diffusion front σ versus time for three different choices of the interaction parameter α.

diffusion front now has a very flat concentration profile; we expect that the limiting situation at which its concentration remains nearly unchanged for all x belonging to the unreacted zone corresponds to the onset of the order–disorder transition in discrete models.

These phenomena can be visually clarified by inspection of the three snapshots of figure 11, where the concentration of A of the profiles of figures 4 and 5 is represented by different

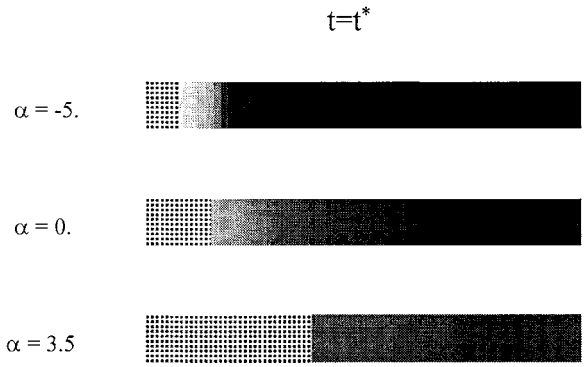

Figure 11. Snapshots of the three different situations studied in the paper: from top to bottom, attractive ($\alpha = -5$), null ($\alpha = 0$) and repulsive interactions ($\alpha = 3.5$) respectively. The values of u are represented in different grey tones. All figures are drawn for the same elapsed time $t^* = 2.1[s]$. The squared area is the region where A has interacted; a depletion zone and a steep profile concentration on the right of the moving interface are present for attractive interactions (upper snapshot). In contrast, an almost uniform grey tone with no depletion layer can be seen for repulsive interaction (lower snapshot).

grey tones that darken at higher concentration of the diffusing species (all pictures are drawn for the same elapsed time). Note the enhancing factor of the repulsive interactions on the interface speed: the interface position, namely, the threshold between the squared area and the grey zone, is shifted more and more to the right for growing α.

The geometric properties of fronts in on-lattice diffusion processes are particularly interesting with respect to the anomalous scaling properties connected with their fractal behaviour. Whatever the criterion introduced to fix the connection between percolating elements [40], a front is a zone that separates a connected network from isolated particles or clusters. With the above considerations in mind, and observing that the advancing speed v of the interface $s(t)$ grows with α (see figures 3 and 11), we focus our attention on the joint inequalities

$$\frac{\partial \sigma}{\partial \alpha} > 0 \cap \frac{\partial v}{\partial \alpha} > 0 \tag{19}$$

where σ can assume the role of 'width of the lattice decay zone'.

Experimentally, it was noted that the growth of layers of binary amorphous alloys is more pronounced in the case of fast diffusion [41]. These situations occur by contact of pure polycrystalline metal or alloys under isothermal conditions. Cases of solid-state amorphization reactions (SSARs) were reported in the presence of repulsive interactions of diffusing species [34].

A simple one-dimensional model cannot capture front anisotropies and local phenomena that seem to have an important role in SSAR [42]. However, it is intriguing to note that, even in the present study, the width of the lattice decay zone σ is greater for high values of v and α that correspond, respectively, to fast diffusion and repulsive interactions.

4. A perturbative approach to the problem

We now propose a perturbative solution of equations (2) and (3) in order to motivate the previously presented numerical results. Very few solutions of moving boundary problems have been obtained by perturbation methods. As pointed out by Crank [29], the analysis is

very complicated and often prohibitive beyond the zero-order approximation. With reference to equations (2) and (3), let us write the dependent variables defining the problem as follows:

$$u = u_0 + \varepsilon u_1 \tag{20}$$

$$s = s_0 + \varepsilon s_1. \tag{21}$$

It is convenient to write the diffusion coefficient in the following form:

$$D = D_0 + \varepsilon f \tag{22}$$

where f depends linearly on concentration, that is $f = ku$.

Inserting equation (20) into (2), we obtain

$$\frac{\partial u_0}{\partial t} + \varepsilon \frac{\partial u_1}{\partial t} = \varepsilon \frac{\partial f}{\partial u} \left(\left(\frac{\partial u_0}{\partial x} \right)^2 + 2\varepsilon \frac{\partial u_0}{\partial x} \frac{\partial u_1}{\partial x} + \varepsilon^2 \left(\frac{\partial u_1}{\partial x} \right)^2 \right) + D_0 \frac{\partial^2 u_0}{\partial x^2} + \varepsilon D_0 \frac{\partial^2 u_1}{\partial x^2} + \varepsilon f \frac{\partial^2 u_0}{\partial x^2} + \varepsilon^2 f \frac{\partial^2 u_1}{\partial x^2}. \tag{23}$$

For the moving interface equation, analogously, we put (21) into (3) and write

$$\frac{\mathrm{d}s_0}{\mathrm{d}t} + \varepsilon \frac{\mathrm{d}s_1}{\mathrm{d}t} = \frac{D(u_\mathrm{i})}{1 - (u_{0\mathrm{i}} + \varepsilon u_{1\mathrm{i}})} \left(\left. \frac{\partial u_0}{\partial x} \right|_\mathrm{i} + \varepsilon \left. \frac{\partial u_1}{\partial x} \right|_\mathrm{i} \right) \tag{24}$$

where the subscript i indicates the values calculated at the moving interface.

Linearizing the first factor appearing on the right-hand side of (24) and collecting the terms according to the exponent of ε, we obtain

$$\frac{\mathrm{d}s_0}{\mathrm{d}t} + \varepsilon \frac{\mathrm{d}s_1}{\mathrm{d}t} \cong \frac{D_0}{1 - u_{0\mathrm{i}}} \left. \frac{\partial u_0}{\partial x} \right|_\mathrm{i} + \varepsilon \frac{k u_{0\mathrm{i}}}{1 - u_{0\mathrm{i}}} \left. \frac{\partial u_0}{\partial x} \right|_\mathrm{i} - \varepsilon \frac{D_0 u_{1\mathrm{i}}}{(1 - u_{0\mathrm{i}})^2} \left. \frac{\partial u_0}{\partial x} \right|_\mathrm{i} + \varepsilon \frac{D_0}{1 - u_{0\mathrm{i}}} \left. \frac{\partial u_1}{\partial x} \right|_\mathrm{i} + \varepsilon^2 \cdots. \tag{25}$$

The zero-order balance, derived from (23) and (25), is

$$\frac{\partial u_0}{\partial t} = D_0 \frac{\partial^2 u_0}{\partial x^2} \tag{26}$$

$$\frac{\mathrm{d}s_0}{\mathrm{d}t} = \frac{D_0}{1 - u_{0\mathrm{i}}} \left. \frac{\partial u_0}{\partial x} \right|_\mathrm{i}. \tag{27}$$

The system of equations (26) and (27) has an explicit solution [33] that reads

$$u_0(x, t) = u_0(0, 0) + [u_0(\infty, 0) - u_0(0, 0)] \operatorname{erf} \left(\frac{x}{2\sqrt{D_0 t}} \right) \tag{28}$$

$$s_0 = \beta \sqrt{D_0 t} \tag{29}$$

where β is a constant pre-factor depending on the boundary conditions.

It is immediate to deduce that the concentration $u_{0\mathrm{i}}$ at the moving interface has a constant value $u_{0\mathrm{i}} = u_{0\mathrm{i}}(\beta)$. This result is consistent with the numerical solution for null interactions ($\alpha = 0 \rightarrow D = D_0$) reported in figure 6.

It is more intriguing to consider the balance of first-order terms in (23) and (25), which assumes the form

$$\frac{\partial u_1}{\partial t} = D_0 \frac{\partial^2 u_1}{\partial x^2} + k \left(\frac{\partial u_0}{\partial x} \right)^2 + k u_0 \frac{\partial^2 u_0}{\partial x^2} = D_0 \frac{\partial u_1}{\partial x^2} + g(x, t) \tag{30}$$

$$\frac{\mathrm{d}s_1}{\mathrm{d}t} = \frac{D_0}{1 - u_{0\mathrm{i}}} \left. \frac{\partial u_1}{\partial x} \right|_\mathrm{i} - \frac{D_0 u_{1\mathrm{i}}}{(1 - u_{1\mathrm{i}})^2} \left. \frac{\partial u_0}{\partial x} \right|_\mathrm{i} + \frac{k u_{0\mathrm{i}}}{1 - u_{0\mathrm{i}}} \left. \frac{\partial u_0}{\partial x} \right|_\mathrm{i}. \tag{31}$$

Let us focus our attention on equation (30), which is a linear equation whose inhomogeneous term, $g(x,t)$, is a known function deriving from the analytical solution of the zero-order perturbative solution. Thus, omitting tedious but straightforward algebraic manipulations, one can show that (30) has a solution u^* depending on the variable $\lambda = x/\sqrt{t}$, namely

$$u_1^* = a_1 \operatorname{erf}\left(\frac{\lambda}{2\sqrt{D_0}}\right) + a_2 + Q(\lambda) \tag{32}$$

where a_1 and a_2 are constant values related to the initial conditions, and $Q(\lambda)$ is a particular solution of the inhomogeneous differential equation.

The system of equations (30), (31) has a solution of the form $s_1 = \gamma\sqrt{D_0 t}$, γ = constant. From the above considerations, we can draw the following conclusions.

(1) From (32), u_{1i} = constant, that is, the concentration value at the travelling interface remains constant as in the zero-order case. This is again consistent with numerical simulations (see figure 6).

(2) $s = s_0 + \varepsilon s_1$ is a linear combination of functions linearly depending on $\sqrt{t}$. It follows that, up to the investigated order, the time evolution of the interface scales with the same law as the linear diffusion process. This result is in agreement with that shown in figure 3, where the position of the interface is plotted versus time in the case of attractive and repulsive interactions.

5. Conclusions

In this work we have presented a study of a diffusive process with moving front and nonlinear diffusivity. The most interesting aspects can be resumed in the following points.

From a methodological point of view, the numerical approach, which takes advantage of a regularization technique, is a further proof of the robustness of the method of Li [36] in revamping the front-tracking algorithms solving moving boundary problems.

Moreover, the results have been compared with simulation data concerning discrete on-lattice models. In particular, an analogy between the present results in the case of strong attractive and repulsive interactions and the physics of phase transitions has been discussed.

Acknowledgment

One of us (APR) is particularly grateful to Miss Deanira Pisana for her kindness and competence in supplying technical support for the realization of this paper.

References

[1] Finlayson B A 1992 *Numerical Methods for Problems with Moving Fronts* (Seattle: Ravenna Park)
[2] Wrobel L C and Brebbla C A (ed) 1993 *Computational Modelling of Free and Moving Boundary Problems* vol 2 (Southampton, Boston: Computational Mechanics)
[3] Dovì V G, Reverberi A P and Meshalkin V P 1994 *Can. J. Chem. Eng.* **72** 1042
[4] Murphy K A 1992 *SIAM J. Control Optim.* **30** 637
[5] Barabàsi A L and Stanley H E 1995 *Fractal Concepts in Surface Growth* (Cambridge: Cambridge University Press)
[6] Family F and Vicsek T 1991 *Dynamics of Fractal Surfaces* (Singapore: World Scientific)
[7] Reverberi A P and Scalas E 1997 *Fractals* **5** 327
[8] Ebert U, van Saarloos W and Caroli C 1997 *Phys. Rev.* E **55** 1530
[9] Ebert U, van Saarloos W and Caroli C 1996 *Phys. Rev. Lett.* **77** 4178
[10] Fife P C 1988 *Dynamics of Internal Layers and Diffusive Iinterfaces* (Philadelphia, PA: Society for Industrial and Applied Mathematics)

[11] Fife P C 1979 *Mathematical Aspects of Reacting and Diffusing Systems (Lecture Notes in Biomathematics vol 28)* (Berlin: Springer)
[12] Benguria R D and Depassier M C 1996 *Phys. Rev. Lett.* **77** 1171
[13] Benguria R D and Depassier M C 1998 *Phys. Rev.* E **57** 6493
[14] Provatas N, Ala-Nissila T, Grant M, Elder K R and Piche L 1995 *J. Stat. Phys.* **81** 737
[15] Lagoudas D C, Entchev P and Triharjanto R 2000 *Comput. Methods Appl. Mech. Eng.* **183** 35
[16] Lagoudas D C and Zhonghai Ding 1998 *Int. J. Eng. Sci.* **36** 367
[17] Gesmundo F and Pereira M 1997 *Oxid. Met.* **47** 507
[18] Nesbitt J A 1995 *Oxid. Met.* **44** 309
[19] Graber R 1999 *Physica* A **271** 223
[20] Reverberi A P and Scalas E 1998 *Physica* A **254** 348
[21] Chopard B, Droz M and Frachebourg L 1994 *Int. J. Mod. Phys.* **5** 47
[22] Sander L M and Ghaisas S V 1996 *Physica* A **233** 629
[23] Goriely A 1995 *Phys. Rev. Lett.* **75** 2047
[24] Powell J and Tabor M 1992 *J. Phys. A: Math. Gen.* **25** 3773
[25] Chopard B, Droz M, Magnin J and Rácz Z 1997 *Phys. Rev.* E **56** 5343
[26] Droz M 1998 *Anomalous Diffusion: from Basics to Applications: Proc. 11th Max Born Symp. (Ladek Zdrój)* p 211
[27] Karma A and Wouter-Jan Rappel 1996 *Phys. Rev.* E **53** R3017
[28] Ihle T and Müller-Krumbhaar H 1994 *Phys. Rev.* E **49** 2972
[29] Crank J 1984 *Free and Moving Boundary Problems* (Oxford: Oxford University Press)
[30] Adrover A and Giona M 1997 *Ind. Eng. Chem. Res.* **36** 2452
[31] van Saarloos W 1998 *Phys. Rep.* **301** 9
[32] Furzeland R M 1980 *J. Inst. Math. Appl.* **26** 411
[33] Wagner C 1952 *J. Electrochem. Soc.* **99** 369
[34] Boyer W S L and Atzmon M 1993 *J. Alloys Compounds* **194** 213
[35] Reverberi A P, Toro L and Vegliò F 2002 *Nonlinear Dynamics and Control in Process Engineering—Recent Advances* ed G Continillo, S Crescitelli and M Giona (Milan: Springer) p 227
[36] Li Z 1997 *Numer. Algorithms* **14** 269–93
[37] Avnir D (ed) 1992 *The Fractal Approach to Heterogeneous Chemistry: Surfaces, Colloids, Polymers* (New York: Wiley)
[38] Kolb M, Gouyet J F and Sapoval B 1987 *Europhys. Lett.* **3** 33
[39] Lepore J R and Albano E V 1998 *J. Chem. Phys.* **108** 5581
[40] Alon U, Balberg I and Drory A 1991 *Phys. Rev. Lett.* **66** 2879
[41] Schwarz R B and Johnson W L 1983 *Phys. Rev. Lett.* **51** 415
[42] Lai W S and Liu B X 1998 *Phys. Rev.* B **58** 6063